Published for SISSA by Springer

Received: *August 13, 2013*
Revised: *October 21, 2013*
Accepted: *October 25, 2013*
Published: *November 5, 2013*

New results on $\nu_\mu \to \nu_\tau$ appearance with the OPERA experiment in the CNGS beam

The OPERA collaboration

E-mail: andrea.longhin@lnf.infn.it, umut.kose@cern.ch

Abstract: The OPERA neutrino experiment is designed to perform the first observation of neutrino oscillations in direct appearance mode in the $\nu_\mu \to \nu_\tau$ channel, via the detection of the τ-leptons created in charged current ν_τ interactions. The detector, located in the underground Gran Sasso Laboratory, consists of an emulsion/lead target with an average mass of about 1.2 kt, complemented by electronic detectors. It is exposed to the CERN Neutrinos to Gran Sasso beam, with a baseline of 730 km and a mean energy of 17 GeV. The observation of the first ν_τ candidate event and the analysis of the 2008-2009 neutrino sample have been reported in previous publications. This work describes substantial improvements in the analysis and in the evaluation of the detection efficiencies and backgrounds using new simulation tools. The analysis is extended to a sub-sample of 2010 and 2011 data, resulting from an electronic detector-based pre-selection, in which an additional ν_τ candidate has been observed. The significance of the two events in terms of a $\nu_\mu \to \nu_\tau$ oscillation signal is of 2.40σ.

Keywords: Oscillation, Neutrino Detectors and Telescopes

ArXiv ePrint: 1308.2553

doi:10.1007/JHEP11(2013)036

JHEP11(2013)036

Contents

1 Introduction

Flavour transitions between neutrino species were predicted nearly 50 years ago [1–3]. In 1998 the Super-Kamiokande experiment observed a strong deficit of atmospheric muon neutrinos in the data, and interpreted it as a result of such transitions [4–6]. A few years later, after being investigated for decades by real-time and geochemical experiments [7–12], the so-called solar neutrino problem could also be interpreted (after the SNO results [13])

JHEP11(2013)036

in terms of neutrino oscillations in presence of the MSW effect [14] in the Sun's matter. The disappearance of ν_μ in atmospheric neutrinos [4–6, 15–17] was confirmed at accelerator-based long baseline experiments [18–20]. The observation of an appearance of neutrinos from oscillations consistent with the disappearance results is still missing. The OPERA experiment [21–24] has the capability of detecting the appearance of a small ν_τ component in a ν_μ beam. The fact that the $\nu_\mu \to \nu_e$ oscillation could not be the dominant reason of the deficit of ν_μ was also established by the measurement of atmospheric ν_e rates and confirmed by nuclear reactor experiments at short baselines [25, 26] in the late nineties. Only recently, the probability amplitude of the $\nu_\mu \to \nu_e$ transition, governed by the θ_{13} mixing angle, has been measured at a long baseline neutrino beam (T2K [27]). The first evidence of the disappearance of $\bar{\nu}_e$ has come from reactor experiments at short baselines and θ_{13} has been measured (Daya Bay [28], Double Chooz [29], RENO [30]). Super-Kamiokande also recently reported a statistical evidence of $\nu_\mu \to \nu_\tau$ transitions [31] in its atmospheric neutrino sample but with a modest signal to background noise due to the difficulty in cleanly reconstructing ν_τ events in a water-Cherenkov detector. A positive evidence from OPERA would definitely prove that the $\nu_\mu \to \nu_\tau$ transition is the reason of ν_μ deficit and it is the dominant mechanism at the atmospheric scale, providing an essential constraint for the establishment of the 3-flavor mixing scheme. Furthermore the measurement can constrain phenomenological models such as neutrino Non Standard Interactions (NSI) [32, 33] or sterile neutrinos, which, for certain choices of the parameters, result in modifications to the expected ν_τ appearance rate.

After two years of technical and low-intensity runs (2006-2007) the OPERA detector in the Gran Sasso underground laboratory (LNGS) has been exposed from 2008 to 2012 to the high-energy CERN Neutrinos to Gran Sasso (CNGS) beam [34–36]. The detection of the first CNGS neutrino interactions in OPERA was reported in [37, 38] and the observation of a first ν_τ candidate event was presented in [39], using a sample corresponding to 1.9×10^{19} protons on target (pot). An update based on the data collected in years 2008-09 (4.88×10^{19} pot) was presented in [40]. This paper presents the progress of the ν_τ appearance search, through a re-evaluation of the efficiencies and of the backgrounds based on a full simulation of the complete analysis chain. Moreover a larger data sample has been exploited which allowed the observation of a second ν_τ candidate event.

After an introduction explaining the operation of the experiment (section 2), the data selection (section 3) and the simulation (section 4), the results (section 5) will be described, giving particular emphasis to the second ν_τ candidate. The significance of the observation of two candidates given the present statistics and the estimated level of background is addressed in section 6 in terms of exclusion of the null-hypothesis.

2 Detector and neutrino beam

The OPERA detector [41] is designed to tackle a challenging task: achieving micro-metric tracking accuracy over a very large detector volume spanning about $(6.5 \times 6.5 \times 8)$ m^3. The scale of the required granularity is set by the flight length of τ leptons, which for the CNGS beam has a roughly exponential distribution with a mean of about 600 μm. This

JHEP11(2013)036

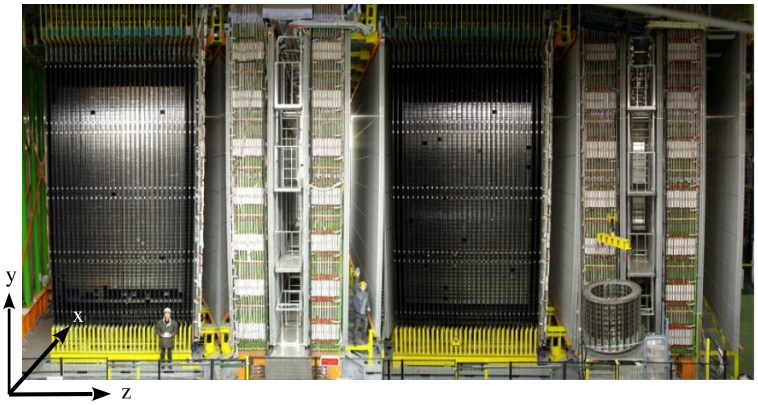

Figure 1. A picture of the OPERA detector. CNGS neutrinos travel from left to right. The (right-handed) reference frame is oriented such that: the y-axis is perpendicular to the hall floor and pointing up; the z-axis is orthogonal to the brick walls and oriented as the incoming neutrinos. The angle between the neutrino direction and the z-axis projected into the yz plane is of 58 mrad.

challenge was addressed by using nuclear emulsion based trackers. Another important constraint is related to the practical impossibility to analyze the full emulsion surface $\mathcal{O}(0.1\ \mathrm{km}^2)$, even with the state-of-the art automatic scanning technology. This, together with other constraints, resulted in a highly modular target made of units based on the Emulsion Cloud Chamber (ECC) technique, hereafter called bricks, interspersed with pair of planes of horizontal and vertical scintillator strips (called Target Tracker or TT [42]) that allow locating with a centimetric resolution the unit in which the neutrino interaction occurred. A brick is composed of 57 emulsion films interleaved with 56, 1 mm thick, lead plates for a mass of 8.3 kg. Its thickness along the beam direction corresponds to about 10 radiation lengths and its transverse size is $128 \times 102\ \mathrm{mm}^2$. A film consists of two 44 μm layers deposited on each side of a 205 μm plastic base. Another key ingredient for the experiment are the Changeable Sheet (CS) doublets [43], attached to the downstream face of each brick. This is a pair of films having received in the underground laboratory a special treatment (refreshing) aiming at erasing most of the cosmic background accumulated since their fabrication. Their scanning allows a relatively fast feedback on the prediction of the electronic detectors (ED) and provides a prediction of the event position in the brick at the $\mathcal{O}(10)\mu$m level, thus greatly helping the vertex location. Finally a magnetic spectrometer system instrumented with Resistive Plate Chamber (RPC) detectors and high-precision Drift Tubes (DT), is used for the task of identifying muons and measuring their charge and momentum. A good muon identification capability is essential to reduce the background to τ decays from charmed particles produced in charged current (CC) ν_μ interactions. The detector (figure 1) is divided into two identical units called Super Modules (SM), each consisting of a target and a spectrometer section. The average number of bricks has been about 140000 for a target mass of about 1.2 kt.

OPERA was exposed to the CNGS ν_μ beam [34–36] at a long-baseline, 730 km away from the source. The neutrino beam, produced by 400 GeV-protons accelerated in the SPS, has an average energy of about 17 GeV, optimised for the observation of ν_τ CC interactions

JHEP11(2013)036

in the OPERA detector. In terms of interactions, the $\bar{\nu}_\mu$ contamination is 2.1%, the ν_e and $\bar{\nu}_e$ contaminations are together below 1%, while the intrinsic ν_τ component (from D_s decays in the CNGS target and beam-dump) is of $\mathcal{O}(10^{-6})$, hence negligible.

3 Data samples and event selection

CNGS completed its operation on December 3, 2012. A sample corresponding to 17.97×10^{19} pot has been registered by the detector since the beginning of the program in 2008. The first task of the electronic detectors DAQ [44] is the time-tagging of the hits allowing the selection of events in coincidence with the two 10.5 μs-wide CNGS spills separated by 50 ms (the so-called "on-time" events).

An on-line filtering (TT local trigger) is then applied in order to remove background from random noise in the detector: hits are required in the horizontal and vertical views of at least two planes or the presence of at least 4 hits in a single plane is required with the sum of their photomultiplier ADC signals exceeding 500 counts (corresponding to about ten photo-electrons).[1]

The event is then classified as being CC-like (hereafter "1μ") or neutral current (NC) like ("0μ") using the data of the target tracker and the spectrometers. Recorded hits are processed by a pattern recognition algorithm and sub-samples of hits in both views are grouped into three dimensional (3D) tracks. A 3D-track is tagged as a muon if the product of its length and the density along its path is larger than 660 g/cm^2. An event is classified as 1μ if either it contains at least one 3D-track tagged as a muon [45] or the total number of TT and RPC planes having at least one hit is larger than 19. The complementary sample is defined as 0μ. About 19% of the NC events are classified as 1μ while only 6% of CC events are classified as 0μ. The momentum of 3D-tracks is calculated from their bending in the spectrometer magnetic field and/or their range with a Kalman filter-based reconstruction algorithm.

A pure sample of 106422 CNGS on-time neutrino interactions is selected (table 1, 3$^{\text{rd}}$ column). About 60% of this sample results from neutrino interactions in the rock in front of the detector typically producing long passing-through muon tracks, while the rest is from interactions occurring, in about equal fractions, in the target (contained events) and in the spectrometer. A classifier algorithm, OpCarac [46], is applied to select the contained events yielding a total of 19505 interactions (table 1, 4$^{\text{th}}$ column). This number corresponds to an average rate of about 18 contained neutrino interactions per day which have been stably recorded with an overall dead-time of the data acquisition and detectors of 1.5%.

Contained events are processed by a brick-finding algorithm [47]. The topology and the energy deposition in the TT scintillator strips, as well as the muon track information (when available) are used to define a three-dimensional probability density map for the vertex position. This probability is integrated over the volumes of the bricks and these are ranked in order of decreasing probability, for extraction and analysis. In the following, the highest-probability brick will be denoted as HPB.

[1] The cut parameters were 10 hits and 30 photo-electrons for 2008 and 2009 runs.

JHEP11(2013)036

year	pot (10^{19})	on-time events	contained events	average No. of bricks
2008	1.74	10141	1931	141475
2009	3.53	21455	4005	147344
2010	4.09	25497	4515	144398
2011	4.75	28195	5131	138798
2012	3.86	21134	3923	135142
all	17.97	106422	19505	141431

Table 1. Summary of the collected data samples. The given pot are corrected for the live-time of the detector. The meaning of the other columns is detailed in the text.

3.1 Brick pre-selection and choice of the analysed sample

The analysis of the 2008-2009 inclusive sample (30% of the overall number of pot) was reported in [40]. In that sample of 2738 fully analysed events one event was recognised as a ν_τ candidate decaying to a single charged hadron (noted as $\tau \to 1h$) [39]. More precisely the measurement of the final state topology and kinematics strongly favors this interpretation: $\tau^- \to \nu_\tau \rho^-$ with $\rho^- \to \pi^- \pi^0$ and $\pi^0 \to \gamma\gamma$.

Since then the scanning strategy has been modified to accelerate the finding of a significant signal for $\nu_\mu \to \nu_\tau$ oscillation. Priority was given to the scanning of a pre-selected sample of bricks:

- 2008-2009 data: analysis of up to two bricks per event without event pre-selection.
- 2010 data: analysis of the HPBs, for all 0μ events and for 1μ events with a muon momentum $p_\mu < 15\,\mathrm{GeV}/c$.
- 2011 data: analysis of the HPBs for all 0μ events.

This pre-selection is temporary and the analysis of lower-priority bricks will occur in the near future.

0μ events form a preferred sample to search for τ decays since these essentially contain signals of the electron final state, with a branching ratio of $(17.85 \pm 0.05)\%$, and of the 1-prong, $(49.52 \pm 0.07)\%$ and 3-prong, $(15.19 \pm 0.08)\%$ hadronic channels.

In the 1μ-decay channel, with a branching ratio of $(17.36 \pm 0.05)\%$, most events occur at low muon momentum. This is due to the fact that the atmospheric-scale oscillation, at this baseline, mainly affects the low-energy region. Moreover, a large fraction of the τ momentum is transferred to the two final-state neutrinos. This is illustrated in the left plot of figure 2 which also shows the distributions of the reconstructed signed muon-momentum ($q \times p_\mu$) for 1μ-events for data and Monte Carlo (MC). The shape of the data is well described by MC, indicating that the pre-selection of events is well understood. The momentum cut at $15\,\mathrm{GeV}/c$ (dashed lines) results in a loss in the sample of muonic τ decays of only 4%. Instead, this cut reduces by 33% the amount of ν_μ^{CC} events to be analysed and, more important, by 28% the size of the charm sample. The momentum cut

JHEP11(2013)036

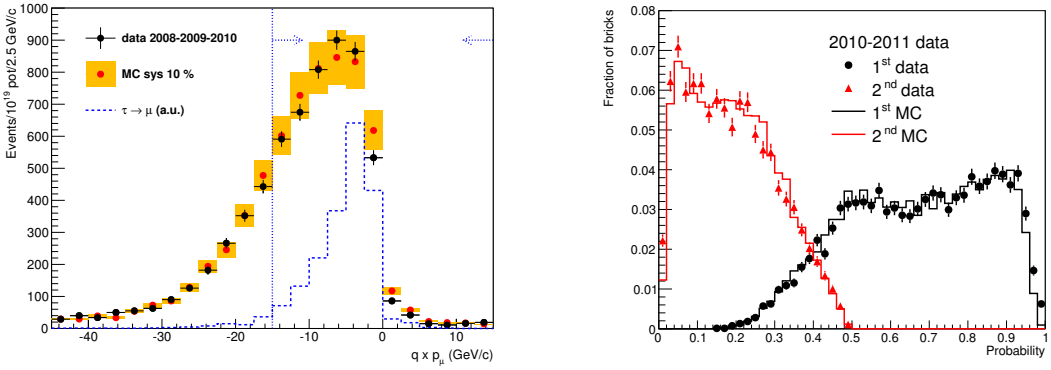

Figure 2. Left: shape comparison of the distributions of the reconstructed muon momentum (p_μ) multiplied by the charge (q) for 1μ events for 2008-2010 data (bullets) and MC (orange band). The pre-selection cut at $\pm$ 15 GeV/c is marked by the vertical lines. The bar height in the MC indicates a 10% systematic error. This uncertainty is related to the knowledge of the CNGS neutrino flux for which we have to rely on the Monte Carlo simulation [45, 48] due to the lack of a near detector constraint. The dashed histogram represents the $\tau \to \mu$ channel MC simulation (shape only). Right: normalized probability distributions for the 1$^{\text{st}}$, 2$^{\text{nd}}$ brick for the data of 2010 and 2011 (bullets) and the MC (histograms).

at 15 GeV/c is also applied to the 2008 and 2009 samples at a later step of the analysis chain in the kinematical selection [23, 24] (see, section 3.5).

The right plot in figure 2 shows the distributions of the brick probability for 0μ and 1μ events of the 2010 and 2011 samples, separately for the first two bricks in the probability ranking. Again, the shape of the brick probability is well described by MC. Details on the MC simulation will be given in section 4.

The number of events selected at the level of electronic detectors (N_{ED}) is 11149 (listed for each year in the first row of table 2). Part of this sample is discarded by the brick finding algorithm based on the topology of the measured hits in the TT. The rejected sample is mainly accounted for by punch-through of external interactions. The numbers of events with a good brick prediction, which are sent to the scanning laboratories (N_{pred}, 9267 in total), are given in the 2$^{\text{nd}}$ row in table 2.

Selected bricks are routinely extracted by a robotic Brick Manipulator System (BMS) capable of keeping up with the average weekly rate of neutrino interactions and thus allowing for the emulsion-based analysis to potentially proceed in parallel to the neutrino interactions data taking. Removed bricks with a negative CS result are re-inserted in the target after replacement of the CS while dismantled bricks are not replaced. Empty spaces are filled by a rearrangement of bricks. This approach aims at keeping the target homogeneous and minimise the occurrence of events with irregularities in the energy flow containment. The position of each brick is registered in a dynamic database to enable the event location.

The average number of bricks in the detector during each run is given in the last column of table 1. The time evolution of the target mass is shown in more detail in figure 3 (blue curve) together with the integrated number of pot (corrected for the inefficiency of

JHEP11(2013)036

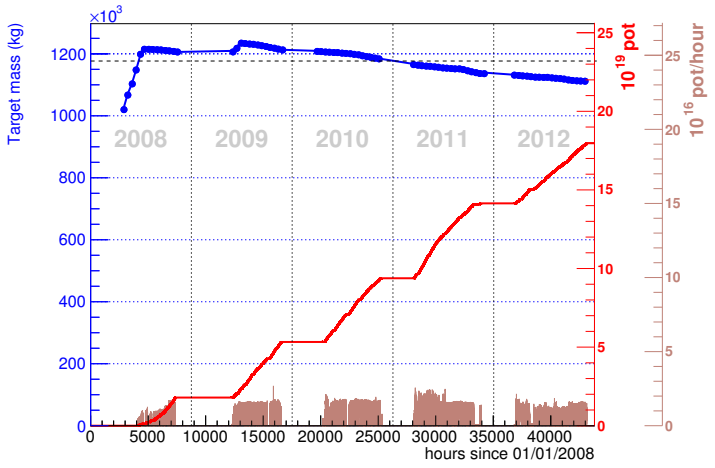

Figure 3. Evolution of the detector target mass (blue bullets) and the integrated number of pot (red line) over the total experiment running. The filled histogram shows the pot in one hour wide bins. The dashed horizontal line shows the pot-weighted average mass which amounts to 1.18 kt.

	2008		**2009**		**2010**		**2011**	**2008-2011**
	0μ	1μ	0μ	1μ	0μ	1μ, $p < 15\,\mathrm{GeV}/c$	0μ	
	2B		2B		1B		1B	all
N_{ED}	552	1379	1199	2806	1420	2109	1684	11149
N_{pred}	404	1328	884	2696	948	2014	993	9267
N_{brick}	152	848	265	1597	218	830	225	4135
N_{DS}	146	819	248	1554	209	794	199	3969

Table 2. Summary of the analysed data samples. 2B stands for two-brick analysis while 1B denotes the highest-probability brick analysis. N_{ED} (section 3.1) are the pre-selected events, N_{pred} (section 3.1) are the events with a brick prediction, N_{brick} (section 3.3) the events located in the bricks and N_{DS} (section 3.4) the number of events for which the decay-search procedure was applied.

the DAQ system, red curve). The loss in target mass at the end of the running amounts to 8.5% of its maximum value.

The pre-selected events (N_{ED}) represent a fraction of 78% and 33% of the 2010 and 2011 contained-event samples, respectively.

3.2 Analysis of the changeable sheets

After the extraction of the selected brick from the detector, the scanning of the CS doublets is performed in order to validate or disprove the brick-finding result. The pattern of tracks reconstructed in the CS doublets can confirm the prediction of the electronic detector, or act as veto and thus trigger the extraction of neighbouring bricks.

CS doublets are inspected by automatic optical scanning microscopes [49–58] in two specialised scanning stations at the LNGS laboratory and at Nagoya University. A rectangular shape is defined centered on the prediction of the electronic detectors with a resulting

JHEP11(2013)036

average scanning area of 20 cm^2 for 1μ events and 35 cm^2 for 0μ events, the pointing accuracy here being poorer due to the absence of a muon track.

The tracking efficiency of the CS doublets has been measured in neutrino data and test beam exposures [43, 59]. A charged particle crossing the CS will produce 4 track segments called micro-tracks. The micro-track detection efficiency for minimum ionising tracks is 95% [59] with the automatic scanning system. The distributions of the residuals in position and angle between the ED and CS tracks have a standard deviation of about 8 mm and 15 mrad respectively.

The analysis and scanning strategy have been improved during the years. In the analysis of the 2008 and 2009 runs, a brick was sent to development as soon as at least one CS track had a possible match with some ED hits. Subsequently the strategy ("CS trigger") has been refined for the 2010 and 2011 runs by requiring the presence of at least:

- for 1μ events, a CS track compatible with the ED muon track within 60 mrad
- for 0μ events, a CS track matching an isolated ED track
- 2 or more CS tracks possibly converging towards a common origin in the brick.

If none of these conditions are fulfilled, the brick is put back in the target with a new CS doublet and the next brick in the probability map is extracted (in case of multi-brick analysis). This method allows saving scanning and analysis time and minimising the target mass loss. In case of a positive outcome, the brick is exposed to cosmic rays in a dedicated pit in the surface LNGS laboratory for 14 hours for high-precision film-to-film alignment, later to be dismantled in the dark room where the emulsion films are developed. The films are finally dispatched to the scanning laboratories of the Collaboration for the "vertex location" and "decay search" analysis.

3.3 Vertex location in the brick

CS tracks are projected to the most downstream emulsion film in the brick (through a distance of about 4.5 mm mainly filled with the plastic and Aluminium film of the CS and brick boxes) where they are searched for. The residuals in position are at the level of 50-60 μm such that the tracks are typically found within the predicted microscope view (400 $\times$ 300 μm). They are then followed upstream film by film ("scan-back" [60, 61]) adjusting the predictions in angle and position at each step to cope with multiple Coulomb scattering (MCS) in the lead plates and measurement errors effects.

The scan-back procedure is stopped when no track candidate is found in three consecutive films; the lead plate just upstream of the last detected segment is defined as the candidate vertex plate. At this stage a volume is defined with a transverse area of 1 cm^2 for 5 films upstream and 10 films downstream of the stopping point (or less if the stopping point lies too upstream or downstream in the brick) and tracks within an angular acceptance $\tan\theta < 0.6$ (θ being the angle of the track with the z axis, figure 1) are searched for in this volume (general scan).

The scan-back procedure is modified for events in which the CS-trigger is produced only by a shower-like topology (mainly due to γ conversions from π^0 decays). In such cases

JHEP11(2013)036

an area of 1 cm^2 centered on the shower axis is analysed for 20 films (corresponding to about 3.5 X_0) starting from the last plate.

All track segments collected in the scanned volumes are analysed by offline algorithms which perform precise alignment, tracking and vertexing. The alignment of the films (with an accuracy of a few μm) is assured by the cosmic ray tracks (section 3.2).

In some cases the scan-back track is not associated to any other track inside the volume due to a low-multiplicity event or because of the angular acceptance limitation or tracking inefficiencies. In this condition the vertex is consider as detected. A further signature of the neutrino interaction can then be obtained from the analysis of nuclear fragments which might be visible in the forward and/or backward hemisphere especially if the interaction happened close to the emulsion layers. Dedicated image analysis tools have been developed [62, 63] to detect highly ionising large-angle tracks in the proximity of the stopping point.

Interactions are tagged as "dead material" when the extrapolated vertex does not lie in the lead plates or in the films (i.e. it is in the scintillator strips, in the brick supporting structure) and no event-related tracks are found in the upstream-brick CS-doublet.

For the 2008-2011 analysed sample, the events located in the brick lead plates ($N_{\rm brick}$) amount to 4135 (table 2).

3.3.1 Data-MC comparison for the location efficiency

An important check of the understanding of the complex task of event location is done at this stage. We consider the data collected in the year 2008 and 2009 and the two-brick analysis strategy.

For the definition of the initial control sample of 0μ events ($N'_{0\mu,ED}$) we adopt a stricter selection on the fiducial volume and a minimal requirement on the energy released in the TT ($E_{TT} > 70\,\text{MeV}$). This allows getting the contamination of external events to the level of 5% in the 0μ sample. This residual contamination has been statistically subtracted. The location efficiency $\epsilon_{\rm loc} = N_{\rm brick}/(N'_{\rm ED}(1-f_{\rm DM})(1-f_{\rm BQ}))$ is then defined, $f_{\rm DM}$ being the fraction of interactions in the dead material which is estimated from the MC simulation ($f_{\rm DM} = 7.8\%$) and $f_{\rm BQ}$ being the fraction of films which could not be analysed due to their bad quality ($f_{\rm BQ} = 6\%$).

The dependence of the location efficiency $\epsilon_{\rm loc}$ on E_{TT} is shown in figure 4 for data and MC for 1μ and for 0μ events. The two quantities are highly correlated in the 0μ sample where the hadronic activity plays a crucial role in the location. The bands in the MC prediction are representing the systematic uncertainty which is 10% for the 1μ sample and the 0μ sample with $E_{TT} > 200\,\text{MeV}$ and 20% for the 0μ sample with $E_{TT} < 200\,\text{MeV}$. The systematic uncertainties account for residual differences in the MC description of the data: the implementation of the CS trigger and brick scanning strategy, the definition of the dead material contribution. For the 0μ sample an additional uncertainty arises from the subtraction of the external background component.

The agreement between data and MC is good in shape and normalisation for the 1μ sample while for the 0μ sample the agreement is good in shape, but data tends to be below the MC by about 15%, independently of E_{TT}. It must be noted, however, that this

JHEP11(2013)036

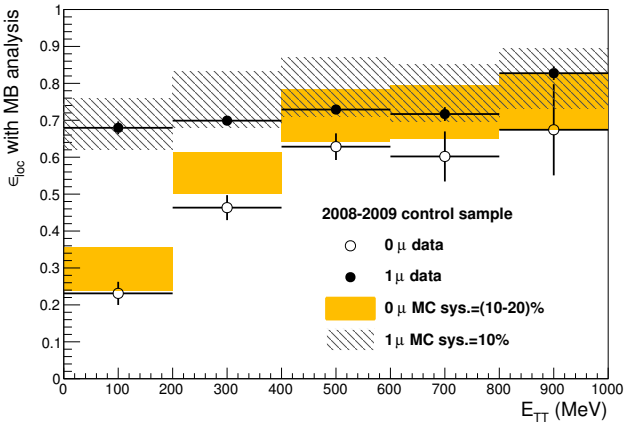

Figure 4. Location efficiency with the two-brick analysis ($\epsilon_{\rm loc}$) vs E_{TT} in a control sample of data collected in 2008 and 2009 (bullets) compared with MC (histograms). The comparison is done separately for 0μ and 1μ events. The error bars represent the systematical and statistical uncertainties in the MC and in the data respectively.

residual difference in the location efficiency in data and Monte Carlo for the 0μ sample has no effect on the predicted signal or background events which is normalised to the number of localised events in the data (see section 4.1).

3.4 Decay search (topological selection)

The decay search (DS) procedure is aimed at detecting the decay topologies of τ leptons produced in ν_τ^{CC} interactions once a vertex has been identified in the volume scan data. The decay is defined as "short" if it happens in the same lead plate where the neutrino interaction occurred or in the first downstream emulsion layer and as "long" if it happens further downstream such that at least one complete micro-track is produced by the τ-lepton. About 46% of the τ decays are expected to be short (43% in the first lead plate and 3% in the first emulsion layer) while the remaining 54% are long decays happening in the first plastic base (11%), in the second emulsion layer (2%), in the second lead plate (25%) or further downstream (16%).

Candidate daughter tracks from short-lived particles decays are selected by requiring their impact parameter (IP) with respect to the reconstructed neutrino interaction vertex to be larger than 10 μm if the depth in lead (λ) is lower than 500 μm or by loosening this requirement to $IP > (5 + 0.01 \times \lambda)$ μm for deeper vertices. The next requirement is that the momentum of the candidate daughter track measured from its MCS (p_{mcs}) [64] is larger than $1\,\mathrm{GeV}/c$. If the number of planes in the scanned volume is not sufficient to estimate p_{mcs} the angular spread S_θ of the available segments is evaluated (see [65] for a detailed definition). If $S_\theta > 15$ mrad in both views, the track is discarded, otherwise the MCS measurement is extended to more plates.

A search is then performed for additional tracks (called extra-tracks) which are not directly connected to the primary vertex: they must be detected in at least 3 films and the distance along the z-axis between the most upstream segment and the neutrino vertex

JHEP11(2013)036

($\Delta z = z_{up} - z_{vtx}$) is required to be positive and less than 3.6 mm. In addition we require $IP < 300$ μm if $\Delta z < 1$ mm and $IP < 500$ μm for $\Delta z > 1$ mm.

In order to deal with topologies in which the first-reconstructed vertex is the decay vertex and thus downstream of the primary neutrino vertex (e.g. in a $\tau \to 3h$ decay) the search for extra tracks is also extended upstream, requiring $\Delta z > -2$ mm and $IP < 500$ μm. For the events located on the basis of a single track (which could be due to a higher-multiplicity decay with tracks outside of the scanning angular acceptance), extra-tracks are searched for within a Δz of $\pm$ 3 mm and $IP < 500$ μm. In this case the z position of the vertex is assumed to be at the center of the lead plate.

A search for charged short-lived parents is then applied to both upstream and downstream extra-tracks by looking for tracks or single segments with $IP < 10$ μm and a distance of closest approach $d_{ca} < 20$ μm with respect to the possible daughter tracks.

Finally the presence of a significant kink (larger than 20 mrad) is checked on the muon track for 1μ events and on all tracks for 0μ events. The four most upstream segments of the track are used to evaluate the ratio (R) between the maximum angular difference between pairs of segments and the overall angular spread [65]. If $R > 5$ then a "kink trigger" is issued and further analysis is performed.

All these operations are supplemented by manual eye-inspection at the microscope in order to improve the information provided by automatic scanning in terms of angular resolution (the automatic system accuracy can sometimes be spoiled by the association of uncorrelated background grains) and efficiency (by recovering the information for inefficient planes). Eye-inspection is also employed to improve the purity by discarding fake tracks (most important for large angles and high-fog[2] films), and furthermore allows excluding passing-through cosmic ray tracks which can mimic extra-tracks due to inefficiencies of the automatic scanning in the five upstream films.

The number of events with a completed decay-search ($N_{\rm DS}$) for the present analysis amounts to 3969 (table 2). This number differs from $N_{\rm brick}$ by about 4% due to the events which fall at the edges of the brick (either in the longitudinal plane or in the transverse direction).

3.4.1 The charm control sample

Given the similarity in mass and decay topologies, the detection of charmed particles constitutes not only a background but also an important tool to verify the understanding of the τ detection efficiency up to the topological selection (decay-search) level.

The charm sample is selected using the same DS analysis as used for the signal search with the exception that the kinematic selection of ν_τ candidate events (which will be described in the following section) is not applied.[3]

The charm yield has been predicted using the latest analysis of the CHORUS data [66] at the WANF neutrino beam ($\langle E_\nu \rangle \simeq 27$ GeV) and re-weighting it for the different neutrino

[2] AgBr crystals can be activated in the emulsion due to thermal or mechanical excitations resulting in the presence of randomly distributed grains which are referred to as "fog".

[3] For 1-prong decays a minimum kink angle of 20 mrad and a momentum of the daughter particle larger than 1 GeV/c is also required.

JHEP11(2013)036

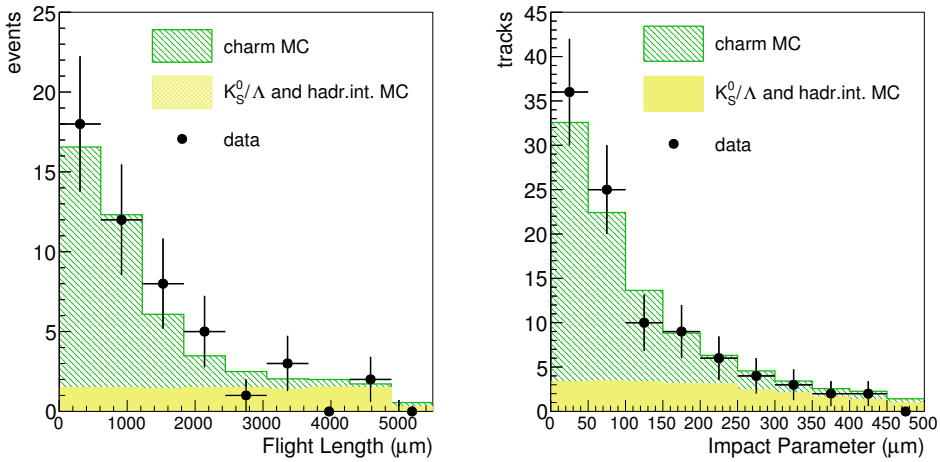

Figure 5. Shape comparison of the distributions of the flight length (left) and the tracks' impact parameters with respect to the primary vertex (right) for the charm data sample of 50 events, described in section 3.4.1, (bullets) and the MC simulation of 40 ± 3 expected charm events (green hatched histogram) and 14 ± 3 expected hadronic interactions and strange meson decays (yellow hatched histograms).

energy spectrum at OPERA (see section 4.2.1 for more details). The decay search efficiency is estimated to be $(58 \pm 8)\%$ for long charm decays and $(18 \pm 2)\%$ for short charm decays. The main sources of background in the charm selection are hadronic re-interactions (about 87% of the total background) and decays of K^0_S or Λ. In the analysed sample of events from the 2008, 2009 and 2010 years having at least a muon tagged 3D-track, a total of (40 ± 3) charm events and (14 ± 3) background events are expected while 50 charm candidate events are observed in the data. The distributions of the flight length of the charm candidates and of the impact parameters of the secondary particles with respect to the primary vertex are presented in figure 5 for data and MC. Not only the absolute yields but also the shapes of the distributions are in very good agreement, which indicates that the systematic error on the estimated efficiency of the full analysis chain cannot exceed 20%. A more extensive discussion of the charm sample will be presented in [67].

3.5 Kinematic selection

Several kinematic quantities of the neutrino interaction are accessible at brick-level via momentum reconstruction using MCS. The energy of electrons and photons is also measured by employing calorimetric techniques [68, 69]. Kinematic criteria can be defined to improve the signal-to-background ratio. To improve the acceptance for electromagnetic showers and reduce the error on the track momentum measurement the standard volume considered for the location (section 3.3) is enlarged and tracks are followed downstream, eventually in other bricks (section 3.6).

After denoting the charged tracks emerging from the neutrino interaction vertex or the decay vertex as "primaries" and "daughters" respectively, and the short-lived primary track as "parent", we define the following relevant variables:

JHEP11(2013)036

- $z_{\rm dec}$: the z-coordinate of the decay vertex with respect to the downstream face of the lead plate containing the primary vertex ($z_{\rm dec} < 44$ μm for short decays).
- p_T^{2ry}: the transverse momentum of the daughter with respect to the parent direction, for 1-prong decays.
- $p_T^{\rm miss}$: the magnitude of the vectorial sum of the transverse momenta of primaries (except the parent) and daughters with respect to the neutrino beam direction.
- p^{2ry}: the scalar sum of the momenta of the daughters.
- $\theta_{\rm kink}$: the average 3D angle between the parent and its daughters (kink angle).
- m: the invariant mass of the daughters (calculated attributing the π mass).
- $m_{\rm min}$: the minimal invariant mass [70].
- ϕ_{lH}: the angle between the parent and the vectorial sum of the other primaries calculated in the plane perpendicular to the CNGS axis.

In the calculation of ϕ_{lH}, if the primary multiplicity (including the τ track candidate) is larger than two, the primaries are defined after removal of the track with the largest difference in ϕ with respect to the τ candidate (TLD) unless it is identified as a hadron with high probability by the track follow-down procedure (section 3.6). This is intended to remove events where the TLD is actually a genuine muon which has not been identified as such by the electronic detectors (for these events, if the TLD would not be excluded the angle would be large and thus the kinematic cut on this variable would not be effective).

The applied selections are summarised for each channel in table 3. The choice of cut parameters has been studied and defined in [23, 24] for the $1h$, electron and muon channels and in [71] for the $3h$ channel.

3.6 Track follow-down

The track kinematics of interesting events fulfilling the selection are further studied in neighbouring bricks. Primary tracks are followed (with an angular acceptance extending up to $\tan\theta = 1$) until either a stopping point, an interaction or a muon decay topology is found (track follow-down, TFD). Thus, by the study of momentum-range correlations, track length, energy loss in proximity of the stopping point, and (if possible) the tagging of interactions or muon decays, a muon/hadron separation exceeding the limitations of the electronic detector reconstruction is obtained.

This procedure results in a significant reduction of the background in all channels from ν_μ^{CC} charm production where the primary μ is not identified in the ED. The TFD technique also provides an important reduction of the background in the $\tau \to \mu$ channel from ν_μ^{CC} events in which the primary μ is wrongly associated to a secondary vertex with a kink topology from a hadronic re-interaction. This also holds for ν_μ^{NC} events with a fake muon. The improved muon/hadron separation provided by TFD is also effective in reducing the

JHEP11(2013)036

variable	$\tau \to 1h$	$\tau \to 3h$	$\tau \to \mu$	$\tau \to e$
lepton-tag	No μ or e at the primary vertex			
$z_{\rm dec}$ (μm)	$[44, 2600]$	< 2600	$[44, 2600]$	< 2600
$p_T^{\rm miss}$ (GeV/c)	$< 1^\star$	$< 1^\star$	/	/
ϕ_{lH} (rad)	$> \pi/2^\star$	$> \pi/2^\star$	/	/
p_T^{2ry} (GeV/c)	$> 0.6(0.3)$*	/	> 0.25	> 0.1
p^{2ry} (GeV/c)	> 2	> 3	> 1 and < 15	> 1 and < 15
$\theta_{\rm kink}$ (mrad)	> 20	< 500	> 20	> 20
$m, m_{\rm min}$ (GeV/c^2)	/	> 0.5 and < 2	/	/

Table 3. Kinematic selection. The meaning of the variables is defined in the text. The cut on p_T^{2ry} for the 1-prong hadronic decay is set at 0.3 GeV/c in the presence of γ particles associated to the decay vertex and to 0.6 otherwise. Cuts marked with a $\star$ are not applied in the case of a QE event. Only long decays are considered for the $\tau \to \mu$ and $\tau \to h$ channels due to a large background component in short decays from charmed particles and hadronic re-interactions respectively.

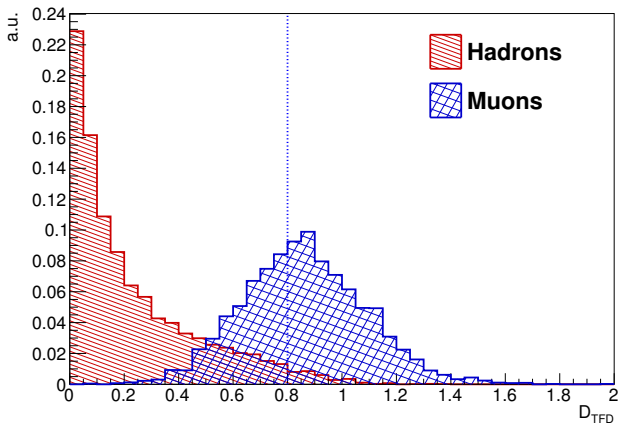

Figure 6. MC distributions of the $D_{\rm TFD}$ variable (section 3.6) used to combine the information on momentum and range to separate muons from hadrons. The red (gray) histograms refers to genuine muons (hadrons). The vertical line denotes the used cut.

background in the hadronic channels due to hadron re-interactions in ν_μ^{CC} events where the electronic detectors alone do not allow the primary μ to be identified unambiguously.

Momentum-range correlations are characterised by a discriminating variable defined as: $D_{\rm TFD} = \frac{L}{R(p)} \frac{\rho}{\langle\rho\rangle}$ where L is the track length, $R(p)$ is the range in lead of a muon with momentum p, $\langle\rho\rangle$ is the average density along the path and ρ is the lead density. The MC distributions of $D_{\rm TFD}$ for hadrons and muons are reported in figure 6. If $D_{\rm TFD} > 0.8$ the track is classified as a muon. Among all the criteria used to separate muons from hadrons, momentum-range correlations and energy loss close to the stopping point, are those having a lower purity in the muon-tagging. For this reason, TLD tracks which are classified by the TFD as hadrons only by one of the above criteria are not included in the calculation of ϕ_{lH}.

JHEP11(2013)036

4 Monte Carlo simulation of signal and backgrounds

Compared to the results published in [40] several improvements have been adopted in the simulation of the detector. Efficiencies and backgrounds are based on a new software framework which combines the information of the electronic and ECC detectors. All particle trajectories are digitised at the micro-track level in a volume consisting of 3×3×3 bricks, with the brick containing the neutrino interaction at the center. For dedicated studies (i.e. for the TFD simulation), also larger volumes have been considered. The efficiency and the resolution (in angle and position) of the scanning microscopes are simulated using parametrisations obtained from real data. The framework allows reproducing the analysis flow from the prioritisation based on the brick probability, the CS-trigger, the CS-to-brick connection, the scan-back, the alignment and the vertexing with full access to the reconstruction parameters. Using this tool the decay search procedure has been included in the efficiency evaluation. Furthermore the detection efficiencies have been re-evaluated for all channels and the simulation of the brick extraction strategies for the different years of data taking has also been updated.

4.1 Expected signal event rates

The neutrino fluxes used in the calculation of the expected signal rates are based on a FLUKA [72, 73] simulation of the CNGS beam-line (2005 revision [74]). The neutrino interactions in the detector are generated using the NEGN generator after a tuning of the parameters based on the high-statistics data sample of the NOMAD experiment [75] . The energy-dependence of the ν_τ cross section that has been used is the default implementantion contained in the GENIE v2.6 simulation program [76]. The $\nu_\mu \to \nu_\tau$ oscillation probability was evaluated using $\Delta m^2_{23} = 2.32 \times 10^{-3}$ eV^2 [77] and $\sin^2 2\theta_{23} = 1$. With these ingredients, the expected rate of ν_τ^{CC} on lead at true level is equal to 3.32 events/(10^{19} pot kt). Taking into account the time evolution of the pot delivery rate and the effective mass of the detector throughout the running period (figure 3) a total number of 66.4 ν_τ CC interactions in lead are expected (with the non-DIS component being about one third [76] of the total).

The expected rate of ν_τ^{CC} events in the 0μ sample can be expressed in terms of the measured event rate in the same category ($n^{0\mu}$ from both ν_μ^{CC} and ν_μ^{NC}) as:

$$n^{0\mu}(\nu_\tau^{CC}) = \frac{n^{0\mu}}{N(\nu_\mu^{CC})} \frac{\langle \epsilon^{0\mu}(\nu_\tau^{CC}) \rangle}{\langle \epsilon^{0\mu}(\nu_\mu^{CC}) \rangle + \alpha \langle \epsilon^{0\mu}(\nu_\mu^{NC}) \rangle} \tag{4.1}$$

denoting with $\langle \epsilon^r(k) \rangle$ the efficiency for reconstructing the process k (ν_μ^{CC}, ν_μ^{NC}) in the reconstructed category r (0μ, 1μ) after convolution with the CNGS flux ϕ; $N(\nu_\mu^{CC})$ being the ν_μ^{CC} interactions at true level and $\alpha = \sigma(\nu_\mu^{NC})/\sigma(\nu_\mu^{CC}) \otimes \phi$. In the present analysis the actual number of $n^{0\mu}$ is taken from the data while other quantities are MC driven. The expected numbers obtained with the above-mentioned procedure are insensitive to systematic effects on the efficiencies up to the location level being common to ν_τ and ν_μ events. The same approach is followed in the prediction of the ν_τ component in the 1μ sample. In this particular case, in addition to the standard 1μ classification (section 3),

JHEP11(2013)036

the presence of a muon tagged 3D track is also required due to the need of matching this ED track to the ECC secondary μ candidate track for the sake of background reduction.

Finally it must be noted that in the present approach the signal efficiency is not taking into account possible migrations between different channels and could therefore be slightly underestimated.

4.2 Expected background event rates

Three sources of backgrounds are giving significant contributions to the final sample: charmed particles decays, hadronic interactions and large-angle muon scattering (LAS). The last one only affects the $\tau \to \mu$ channel while the other classes differently affect all decay channels. These backgrounds have been discussed extensively in [23, 24]. The basic ingredients for the more recent evaluation of these components will be discussed in the following.

4.2.1 Charmed particle decays

The most effective tool for the rejection of the background from charmed particles is an efficient identification of the primary muon in ν_μ^{CC} interactions. The fraction of ν_μ^{CC} events having an associated charm quark at the CNGS energies is estimated from the CHORUS measurement [66] as $(\sigma(\nu_\mu^{CC} + c)/\sigma(\nu_\mu^{CC})) \otimes \phi = (4.38 \pm 0.26)\%$. The tagging of the primary muon is achieved first, at the level of the ED, via the reconstruction of penetrating 3D-tracks and the vetoing of events involving many TT planes (to complement the tracking) as described in section 3. Requiring an event to be classified as 0μ reduces the yield down to 6% of the initial charm sample. At the emulsion detector level, the TFD procedure gives a further suppression by 60%. Taking into account the effects of the full analysis chain and considering only the HPB, an overall suppression of 3.3×10^{-5} is obtained in the $1h$ channel and 3.4×10^{-4} in the $3h$ channel. The two-brick analysis gives an increase by a factor 20-25% resulting in an expectation of 0.027 ± 0.005 events and 0.12 ± 0.02 events in the analysed sample for the $1h$ and $3h$ channels respectively (figure 7, green-coloured histogram and table 4).

The background from charmed particles in the $\tau \to e$ decay channel (where, unlike in the muon case, the positive charge of the decay electron cannot be measured) gives a contribution in the analysed sample of 0.020 ± 0.004 events. This is the only significant background in this channel.

The background from charmed particles in the $\tau \to \mu$ decay channel is relatively small since it only arises in two cases i.e. 1) when the primary μ is not identified, a muonic decay occurs ($f(C^+ \to \mu^+ h^0) = (5.3 \pm 2.8)\%$), and the positive charge of the secondary μ is not measured or mis-identified; 2) the secondary μ is not identified and the primary μ is wrongly matched to the decay daughter. This results in a background contribution of 0.011 ± 0.005 events (figure 7, green-coloured histogram and table 4).

Finally, the double charm production in NC interactions process has to be considered. The yield has been measured by the CHORUS collaboration to be $\sigma(c\bar{c}\nu)/\sigma_{NC}^{DIS} = (3.62^{+2.9}_{-2.4}(\text{stat.}) \pm 0.54(\text{sys.})) \times 10^{-3}$ [78]. This component cannot profit of the suppression given by the primary muon identification but, on the other hand, it can be removed by

JHEP11(2013)036

measuring the presence of the primary and secondary vertices. This contribution, which is expected to be a second order correction, is not included in the present estimates.

The uncertainty on the charm background component is estimated within the 20% level based on the measured sample of charm events (section 3.4.1).

4.2.2 Hadronic re-interactions.

This background has been estimated by giving hadronic tracks from located 0μ events (from an initial sample of 9×10^6 ν_μ^{NC} interactions) as an input to a FLUKA-based MC simulation. With respect to a similar analysis reported in [40] this approach implements the FLUKA hadronic models to fully reconstructed events thus including the biases introduced by the selection chain, up to the event-location level.

The fraction of located 0μ events with at least one track mimicking the topology of a single-prong long decay and $\theta_{\rm kink} > 20$ mrad is found to be 2.1% while the fraction with at least a track producing three visible prongs in the scanning acceptance is 0.18% (short and long). The kinematic selection (in particular the p^{2ry} and p_T^{2ry} cuts) strongly reduces the "topological" sample to $(0.27 \pm 0.02(\text{stat.}))\%$ $(1h)$ and $(1.2 \pm 0.1(\text{stat.}))\%$ $(3h)$, due to the typical low transverse momentum of the secondary products. At this stage an additional reduction of 30% is obtained by requiring the absence of nuclear fragments (either in the backward or forward hemisphere) or minimum ionising particles up to $\tan\theta = 3$. Finally the estimated rate of background events amounts to $(3.9 \pm 0.2(\text{stat.})) \times 10^{-5}$ of the located 0μ events for the $1h$ channel and $(1.5 \pm 0.2(\text{stat.})) \times 10^{-5}$ for the $3h$ channel. The expected interaction rate per unit length in the plastic base is about 4.5 times smaller than in the lead plate due to the combined effect of the density and the mean atomic number.

Several data-driven checks of the FLUKA description of hadronic interactions in the OPERA bricks were performed [40]. In general a good agreement between data and simulation is observed for different data-sets: a sample of hadronic interactions of pions of 2, 4 and 10 GeV/c momenta from a CERN-based test beam; a sample of hadronic tracks from CNGS neutrino interactions measured in the emulsions (total length 19 m) and a sample of hadronic nuclear fragments from test-beam pion interactions for which the yields and angular distributions have been studied. With respect to [40], analyses based on larger data samples have been developed [79–82] allowing estimating an accuracy of the predictions for the hadronic background at the 30% level. The uncertainty in the rate of high-angle nuclear fragments emitted in hadronic re-interactions is estimated in [82] at the 10% level. In conclusion, considering the $1h$ and $3h$ channels together, in the analysed sample a total of 0.018 ± 0.005 events from hadronic re-interactions is expected (figure 7, yellow-coloured histogram and table 4).

4.2.3 Large-angle muon scattering.

The occurrence of large-angle scattering of muons in thin ($\mathcal{O}(0.1)X_0$) lead plates is, at present, not well constrained by measurements. Upper limits from extrapolations of measurements on copper or nuclear emulsions have been reported in [23, 24]: the rates in the signal region $\theta_{\rm kink} > 20$ mrad and $p_T^\mu > 0.25$ GeV/c for muon tracks with a realistic angular and momentum spectrum, are, at 90% C.L., $< 2.3 \times 10^{-5}$ and $< 4.1 \times 10^{-5}$, respectively.

JHEP11(2013)036

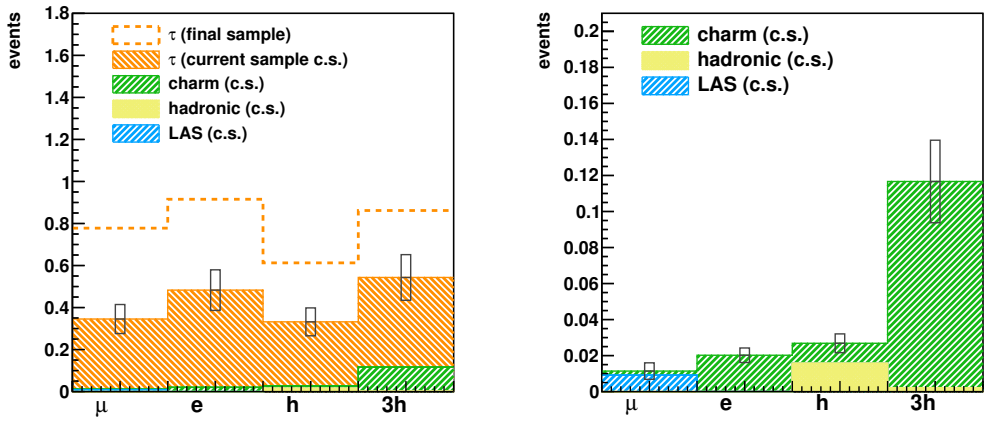

Figure 7. Signal and backgrounds (left panel) and backgrounds only (right panel) expectations by channel for the sample considered in this paper ("c.s.", filled histograms). Black rectangles show the estimated uncertainty. The dashed line in the left plot shows the signal expectation for the two-brick analysis of the complete data sample collected in the year 2008-2012.

	Signal events $\Delta m^2_{23} = 2.32\text{m}(\text{eV}^2)$	All backgrounds	Charm background	LAS background	Hadronic background
$\tau \to h$	0.31 ± 0.06	0.027 ± 0.005	0.011 ± 0.002	/	0.016 ± 0.005
$\tau \to 3h$	0.43 ± 0.09	0.12 ± 0.02	0.11 ± 0.02	/	0.0021 ± 0.0006
$\tau \to \mu$	0.33 ± 0.07	0.011 ± 0.005	0.0023 ± 0.0004	0.009 ± 0.005	/
$\tau \to e$	0.46 ± 0.09	0.020 ± 0.004	0.020 ± 0.004	/	/
all	1.53 ± 0.16	0.175 ± 0.024	0.15 ± 0.02	0.009 ± 0.005	0.018 ± 0.005

Table 4. Signal and backgrounds expectations for the analysed sample. The numbers correspond to the filled histograms in figure 7.

A dedicated measurement of large angle scattering of 9 GeV/c muons from thin lead plates is also reported in [23, 24] giving $0.6^{+0.7}_{-0.6} \times 10^{-5}$. A GEANT 3.21 [83] based simulation, modified to take into account data on the nuclear form factor of lead and inelastic interactions, predicts a rate of 2×10^{-6}. More experimental activities to determine this process are in progress. In the present work the same contribution used for the experiment proposal [23, 24] (1×10^{-5}) is assumed corresponding to 0.009 ± 0.005 events in the analysed sample (figure 7, blue-coloured histogram and table 4).

4.2.4 Summary of the expected event numbers.

The estimated signal and background events for the sample considered in the present analysis are summarised in a graphical form in figure 7, for each decay channel and in tabular form in table 4. The background from charmed particles is the dominant one in the $\tau \to e$ and $\tau \to 3h$ channels while LAS in the $\tau \to \mu$ channel and hadronic re-interactions in the $\tau \to 1h$ channel are the largest backgrounds. The systematic uncertainty on the signal and on the charm background is estimated to be 20% (section 3.4.1) and the one on

JHEP11(2013)036

the hadronic background to be 30%. The LAS background uncertainty is assumed to be of the order of 50% (grey bars in figure 7).

The expectation for the signal events using the two-brick analysis in the final data sample (2008-2012) is of 3.2 ± 0.3 observed ν_τ events (dashed line in figure 7, left). This number is calculated using $\Delta m^2_{23} = 2.32 \times 10^{-3}\text{eV}^2$ as a central value,[4] the accumulated statistics of 17.97×10^{19} pot and a dynamic target mass (figure 3) corrected for the dead material and the fraction of bad-quality films (section 3.3). Furthermore this estimate is based on a realistic simulation of all the steps of the analysis chain and in particular the decay search phase (section 3.4) which had not been simulated in full detail in previous analyses.

The current estimate does not include some factors which are expected to increase the efficiency. The extension of the analysis to the 3$^{\text{rd}}$ and 4$^{\text{th}}$ bricks in the probability map is foreseen. Smaller effects due to the migration of ν_τ events from one channel to another are not taken into account at present. These effects increase only the expected number of ν_τ events, while keeping the background at the same level. Finally an optimisation of the selection is ongoing within the new simulation framework with the goal of maximising the expected sensitivity.

5 Analysed sample and results

The number of events from the present analysed sample surviving the complete selection chain described above amounts to two τ-candidates (hereafter called A and B). Given that the candidate which occurred first (A, $\tau \to 1h$) has already been extensively documented in [39, 40], this paper will focus on the description of the second candidate.

5.1 Description of the second ν_τ candidate event

This neutrino interaction occurred on 23 April 2011 at 7.15 UTC time. The pattern of hit scintillator strips in the TT is shown in figure 8. The event, of which the estimated hadronic energy is (22.0 ± 6.2) GeV, is classified as 0μ and the bulk of the activity in the electronic detector is contained within about 6 to 8 brick walls (more than 60 X_0 and about 2.5 pion interaction lengths). The interaction took place in the target of the upstream Super Module and lies well within the brick-filled target region. The neutrino vertex brick (having a probability of 63%) was located in the longitudinal direction (z), in the second most upstream brick layer (called W_0), in the horizontal direction (x), in the 3$^{\text{rd}}$ brick layer from the closest side (left side looking towards the CNGS) and, in the vertical direction (y), in the 19$^{\text{th}}$ brick layer from the bottom. In figure 8 the position of the brick containing the interaction is highlighted. A linear extrapolation of the vertex tracks found in the emulsions (described in the following) is also shown to illustrate the matching with hits in the scintillators. The event emulsion data has been independently measured with the European and Japanese scanning systems with consistent results. The average values are considered in the following. The interaction is well inside the brick in the longitudinal coordinate lying slightly upstream of the center of the brick (22$^{\text{nd}}$ lead plate in increasing

[4] The number of oscillated events has a quadratic dependence on Δm^2_{23}.

JHEP11(2013)036

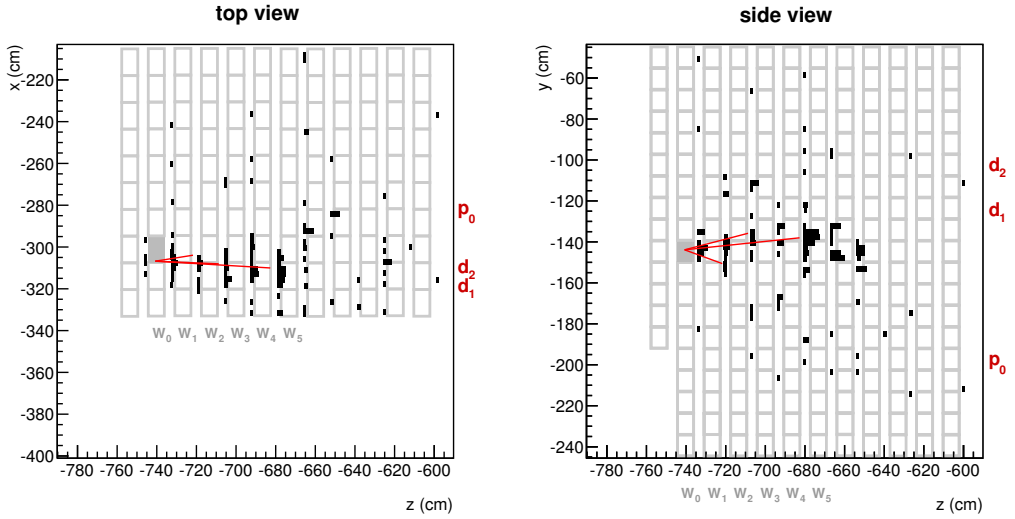

Figure 8. Event display of ν_τ candidate event B: Target Tracker hits with brick tracks superimposed. The left panel is the top-view, the right panel the side-view. The position of the brick containing the neutrino interaction is highlighted.

z order) while in the transverse plane it lies at 6.8 mm and 41.4 mm from the closest sides in x and y.

The topology of the primary vertex (V_0 in figure 9) consists of two tracks, the τ lepton candidate and another track (called p_0). The distance of closest approach of the p_0 and τ tracks equals to 0.2 μm and the vertex lies close to the downstream emulsion film, at a depth in lead of only 120 μm. A forward-going nuclear fragment associated to the primary vertex has also been detected at a large angle with slopes of: $(1.15, -0.28)$.[5]

The flight length of the τ lepton candidate is (1466 ± 10) μm and its decay occurs in the plastic base allowing excluding with a high efficiency (above 99.8% at 90% C.L. up to $\tan\theta = 3$, [62]) the emission of highly ionising nuclear fragments. The secondary vertex (V_1, figure 9) consists of three tracks (called d_1, d_2, d_3). A display of the reconstructed grains in the emulsion layers is presented in figure 10. The impact parameters of the decay products with respect to the reconstructed secondary vertex are 1.3, 1.2 and 0.3 μm for d_1, d_2 and d_3 respectively. After eye-inspection the background from instrumental fake tracks or tracks due to Compton electrons is negligible.

In the beam transverse plane the τ and the p_0 tracks form an angle $\Delta\phi_{\tau H} = (167.8 \pm 1.1)^\circ$ (figure 11).

In order to strongly constrain the hypothesis that the secondary vertex could be a hadronic interaction, a search for nuclear fragments has been performed both upstream and downstream of the vertex with an automatic scanning up to $\tan\theta = 3.5$ as well as by visual inspection. No such fragment was found.

A search for γ conversions has been performed up to $\tan\theta = 1$ for the 35 films (about 6 X_0) downstream of the vertex yielding no candidates.

[5]Slopes are given as tangents of the projected angles after correction for the 58 mrad vertical tilt of the beam.

JHEP11(2013)036

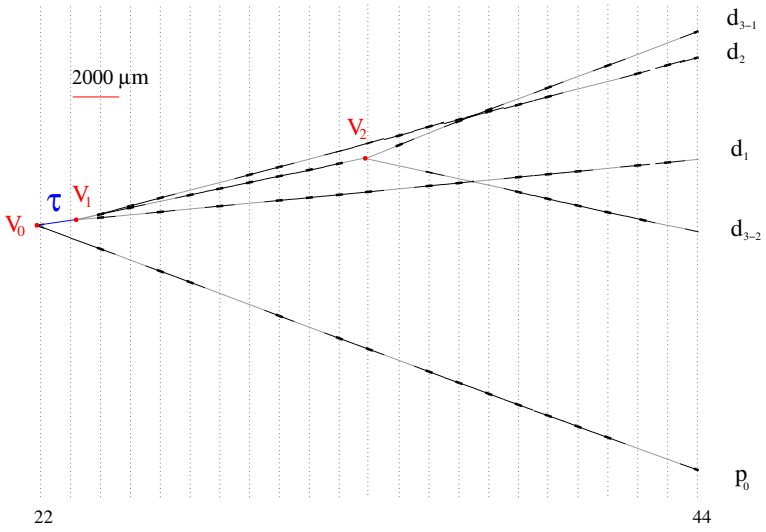

Figure 9. Event display of ν_τ candidate event B: reconstruction in the brick (side-view). Vertical lines indicate the position of the middle-point of emulsion films 22 to 44, numbering them in order of increasing z from 1 to 57. The pitch is 1.3 mm. The black segments represent reconstructed base-tracks while the gray lines are the result of the track fit.

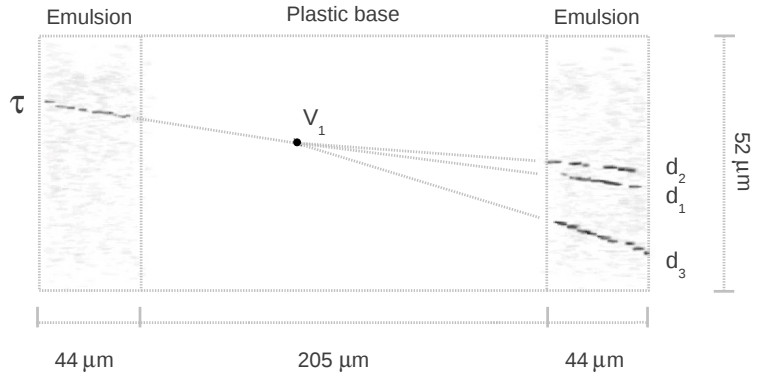

Figure 10. Top-view display of the candidate $\tau \to 3h$ decay vertex (V_1 in figure 9). The single grains observed by the optical microscope are visible in the emulsion layers (left-side and right-side rectangles). The directions of micro-tracks are extrapolated to the decay vertex in the plastic base region (central rectangle).

The analysis of each track to determine its nature and momentum is described below:

- track p_0 has a measured momentum $p_{p_0} = (2.8^{+0.7}_{-0.7})\,\mathrm{GeV}/c$. This track points towards the centre of the detector in the top-view such that its signature as a hadron is already well constrained using the target tracker information only. Nevertheless the track has been followed in the downstream wall (W_1) where it is found to exit the brick to the side. Compatible tracks have neither been found in the adjacent brick in W_1 nor in downstream bricks (and CS doublets) up to W_3. Gamma rays from a possible hadronic interaction were also searched for in two bricks in W_2, however, no

JHEP11(2013)036

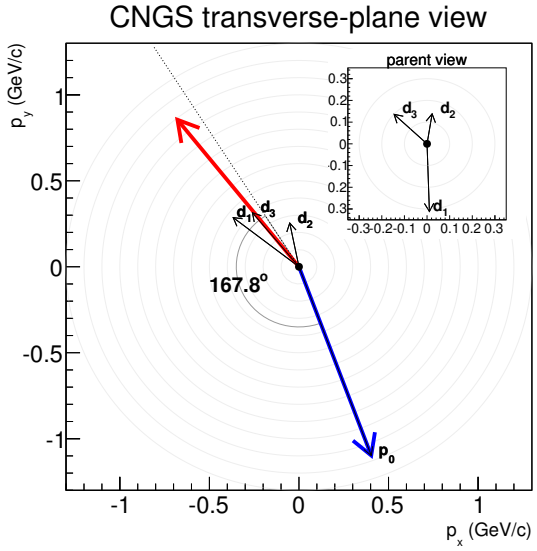

Figure 11. Event display of ν_τ candidate event B: CNGS transverse plane momentum balancing. The red (blue) line represents the sum of the transverse momentum of the secondary (primary) vertex tracks. The dotted line marks the direction of the parent. The inset represents the transverse momenta of daughter tracks along the parent flight length direction.

γ was found. This track is then assumed to interact in the dead material in-between two bricks. A muon with a momentum of the magnitude measured by MCS would be expected to travel from 26 to 44 brick layers before stopping. This makes the muon hypothesis very unlikely: D_{TFD} is 0.05 for this track. Its projected slopes are $(0.155, -0.365)$, well inside the angular acceptance of the scanning. Even considering the possibility of having missed a muon track crossing the downstream emulsion detectors, the pattern in the scintillators does not allow the existence of such a track for more than about 7-8 brick walls.

- track d_1 has slopes of (-0.056, 0.101) and a measured momentum $p_{d_1} = (6.6^{+2.0}_{-1.4})\,\mathrm{GeV}/c$. A hadronic interaction is detected in the emulsions of the brick in wall W_4 (see figure 8) producing two charged tracks with slopes of (0.234, 0.489) and (0.034, -0.305). The signature of the interaction is also indicated by the target tracker scintillators.

- track d_2 has a slope of (-0.041, 0.260) and a measured momentum $p_{d_2} = (1.3^{+0.2}_{-0.2})\,\mathrm{GeV}/c$. It has not been found in W_2 or in the following walls corresponding to a range-momentum correlation parameter $D_{\mathrm{TFD}} = 0.25$.

- track d_3 has a slope of (-0.134, 0.220) and a measured momentum $p_{d_3} = (2.0^{+0.9}_{-0.6})\,\mathrm{GeV}/c$. This track interacts in the brick containing the neutrino vertex, after 11 lead plates i.e. about 1.3 cm downstream (V_2 in figure 9). The interaction occurs inside the emulsion resulting in a very clear signature. The final state is composed of two charged tracks (d_{3-1} and d_{3-2}) and four back-scattered nuclear fragments.

The scalar sum of the momenta of all the measured charged particles in the event is $12.7^{+2.3}_{-1.7}\,\mathrm{GeV}/c$.

JHEP11(2013)036

Variable	$\tau \to 1h$ selection	candidate event A	$\tau \to 3h$ selection	candidate event B
$z_{\rm dec}$ (μm)	< 2600	435 ± 35	idem	1446 ± 10
ϕ_{lH} (°)	> 90	172.5 ± 1.7	idem	167.8 ± 1.1
$\langle\theta_{\rm kink}\rangle$ (mrad)	> 20	41 ± 2	< 500	87.4 ± 1.5
$p_T^{\rm miss}$ (GeV/c)	< 1	$0.57^{+0.32}_{-0.17}$	idem	0.31 ± 0.11
p_{2ry} (GeV/c)	> 2	12^{+6}_{-3}	> 3	8.4 ± 1.7
$p_{T,2ry}$ (GeV/c)	$> 0.3(0.6)$	$0.47^{+0.24}_{-0.12}$	/	/
$m_{\rm min}$ (GeV/c^2)	/	/	[0.5, 2]	0.96 ± 0.13
m (GeV/c^2)	/	/	[0.5, 2]	0.80 ± 0.12

Table 5. Selection criteria for ν_τ candidate events and corresponding measured values.

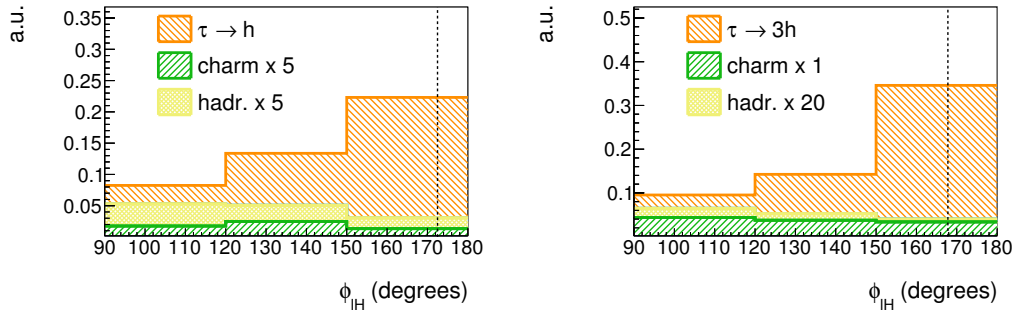

Figure 12. Distributions of ϕ_{lH} for the $\tau \to 1h$ (left) and $\tau \to 3h$ (right) selections. The filled histograms represent in different colors (see the legend) the MC expectation for signal and background while the vertical lines represent the values measured for the τ candidates. The background and signal components are stacked and, for the sake of visualisation, backgrounds have been scaled up with the factors indicated in the legends.

5.2 Summary of the two ν_τ candidate events

From the arguments developed in [39, 40] and in section 5.1, it is concluded that the two events are candidates of τ decays into the 1-charged hadron ($1h$) and 3-charged hadrons ($3h$) channels, respectively. table 5 summarises the values taken by the kinematic variables for the two candidates together with the cuts applied in the analysis. The distributions of ϕ_{lH}, for the expected signal and background components in the analysed sample are presented in figure 12 for the $1h$ and $3h$ channels separately. The measured values in the data are indicated by vertical lines.

6 Significance of the observation

The significance of the observation of two candidates with the present estimate of the backgrounds is addressed by considering the confidence in the exclusion of the null hypothesis (i.e. having observed no $\nu_\mu \to \nu_\tau$ oscillation signal). The probability that the two events

JHEP11(2013)036

might be due to an upward fluctuation of the background is defined as the integral of the Poisson distribution evaluated for $n \geq 2$: $p = \sum_{n=2}^{\infty} \mu^n \frac{e^{-\mu}}{n!}$. Using for μ the sum of the background in the four channels (see figure 7), the value $p = 1.36 \times 10^{-2}$ is obtained, corresponding to a 2.20σ exclusion (adopting the one-sided definition).

In a similar manner the p-values of the two channels can be defined: $p_{1h} = 2.6 \times 10^{-2}$ (1.94σ) and $p_{3h} = 1.10 \times 10^{-1}$ (1.23σ). To combine them, an approach based on generating a large number of pseudo-experiments has then been followed. For each of the four τ decay channels an integer, $n_{i=1,\ldots,4}$, is extracted from the Poisson distribution of background. The p_i values are then calculated as above for each extraction and the estimator of the results $p^\star$ is obtained by taking their product $p^\star = p_1 p_2 p_3 p_4$ (different choices of estimator exist). The counting of the fraction of pseudo experiments for which $p^\star \leq p_{1h} p_{3h}$ yields a significance of 2.40σ. More elaborated estimates of the significance could be obtained using a log-likelihood ratio analysis or other multi-variate techniques. This approach will be addressed in future works.

7 Conclusions and prospects

The results of the ν_τ appearance analysis on a pre-selected sample of the neutrino interactions collected by the OPERA experiment in the years 2008 to 2011 are reported. A two-brick analysis was performed on all 2008 and 2009 predictions while for 2010 and 2011 the analysis was restricted to the most probable brick of all 0μ events and of 1μ events with $p_\mu < 15\,\mathrm{GeV}/c$ of the 2010 sample. In terms of expected signal events the considered sample corresponds to about 50% of the final expectation. A total of two ν_τ candidates has been observed, one in the $\tau \to 1h$ channel and one in the $\tau \to 3h$ channel. This result is compatible with the expected amount of 1.53 ± 0.16 signal events and 0.18 ± 0.02 background events in all channels. The good agreement between data and MC, both for the location efficiencies of ν_μ events and for the detection of charmed particles, indicates that the overall τ finding efficiencies are well understood. Using the presently analysed sample the absence of a signal from $\nu_\mu \to \nu_\tau$ oscillations (null hypothesis) is excluded at 2.40σ.

In the near future, the analysis of the 2011 sample will be completed using the same event selection as for 2010 as well as that of the 2012 sample currently in progress. Finally the search for events not found in the HPB will be extended to second-priority bricks as it was done for the 2008 and 2009 samples. The inclusion of 3$^{\mathrm{rd}}$ and 4$^{\mathrm{th}}$ bricks, which is also foreseen as a further step, will bring an additional increase of the location efficiency. The current significance can be improved with the ongoing increase of the analysed sample.

Acknowledgments

We thank CERN for the successful operation of the CNGS facility and INFN for the continuous support given to the experiment during the construction, installation and commissioning phases through its LNGS laboratory. We warmly acknowledge funding from our national agencies: Fonds de la Recherche Scientifique-FNRS and Institut InterUniversitaire des Sciences Nucléaires for Belgium, MoSES for Croatia, CNRS and IN2P3

JHEP11(2013)036

for France, BMBF for Germany, INFN for Italy, JSPS (Japan Society for the Promotion of Science), MEXT (Ministry of Education, Culture, Sports, Science and Technology), QFPU (Global COE programme of Nagoya University, Quest for Fundamental Principles in the Universe supported by JSPS and MEXT) and Promotion and Mutual Aid Corporation for Private Schools of Japan for Japan, SNF, the University of Bern and ETH Zurich for Switzerland, the Russian Foundation for Basic Research (grant no. 09-02-00300 a, 12-02-12142 ofim), the Programs of the Presidium of the Russian Academy of Sciences Neutrino physics and Experimental and theoretical researches of fundamental interactions connected with work on the accelerator of CERN, the Programs of Support of Leading Schools (grant no. 3517.2010.2), and the Ministry of Education and Science of the Russian Federation for Russia, the National Research Foundation of Korea Grant No. 2011-0029457 for Korea and TUBITAK, the Scientific and Technological Research Council of Turkey, for Turkey. We are also indebted to INFN for providing fellowships and grants to non-Italian researchers. We thank the IN2P3 Computing Centre (CC-IN2P3) for providing computing resources for the analysis and hosting the central database for the OPERA experiment. We are indebted to our technical collaborators for the excellent quality of their work over many years of design, prototyping and construction of the detector and of its facilities.

References

[1] B. Pontecorvo, *Mesonium and anti-mesonium*, *Sov. Phys. JETP* **6** (1957) 429 [INSPIRE].

[2] B. Pontecorvo, *Inverse β processes and nonconservation of lepton charge*, *Sov. Phys. JETP* **7** (1958) 172 [INSPIRE].

[3] Z. Maki, M. Nakagawa and S. Sakata, *Remarks on the unified model of elementary particles*, *Prog. Theor. Phys.* **28** (1962) 870 [INSPIRE].

[4] Super-Kamiokande collaboration, Y. Fukuda et al., *Evidence for oscillation of atmospheric neutrinos*, *Phys. Rev. Lett.* **81** (1998) 1562 [hep-ex/9807003] [INSPIRE].

[5] Super-Kamiokande collaboration, K. Abe et al., *A measurement of atmospheric neutrino flux consistent with tau neutrino appearance*, *Phys. Rev. Lett.* **97** (2006) 171801 [hep-ex/0607059] [INSPIRE].

[6] Super-Kamiokande collaboration, R. Wendell et al., *Atmospheric neutrino oscillation analysis with sub-leading effects in Super-Kamiokande I, II and III*, *Phys. Rev.* **D 81** (2010) 092004 [arXiv:1002.3471] [INSPIRE].

[7] Super-Kamiokande collaboration, S. Fukuda et al., *Constraints on neutrino oscillations using 1258 days of Super-Kamiokande solar neutrino data*, *Phys. Rev. Lett.* **86** (2001) 5656 [hep-ex/0103033] [INSPIRE].

[8] SAGE collaboration, J. Abdurashitov et al., *Solar neutrino flux measurements by the Soviet-American Gallium Experiment (SAGE) for half the 22 year solar cycle*, *J. Exp. Theor. Phys.* **95** (2002) 181 [astro-ph/0204245] [INSPIRE].

JHEP11(2013)036

[9] GALLEX collaboration, W. Hampel et al., *GALLEX solar neutrino observations: Results for GALLEX IV*, *Phys. Lett.* **B 447** (1999) 127 [INSPIRE].

[10] GNO collaboration, M. Altmann et al., *Complete results for five years of GNO solar neutrino observations*, *Phys. Lett.* **B 616** (2005) 174 [hep-ex/0504037] [INSPIRE].

[11] KamLAND collaboration, S. Abe et al., *Precision measurement of neutrino oscillation parameters with KamLAND*, *Phys. Rev. Lett.* **100** (2008) 221803 [arXiv:0801.4589] [INSPIRE].

[12] Borexino collaboration, C. Arpesella et al., *Direct measurement of the Be-7 solar neutrino flux with 192 days of Borexino data*, *Phys. Rev. Lett.* **101** (2008) 091302 [arXiv:0805.3843] [INSPIRE].

[13] SNO collaboration, Q. Ahmad et al., *Measurement of the rate of $\nu_e + d \to p + p + e^-$ interactions produced by B-8 solar neutrinos at the Sudbury Neutrino Observatory*, *Phys. Rev. Lett.* **87** (2001) 071301 [nucl-ex/0106015] [INSPIRE].

[14] A.Y. Smirnov, *The MSW effect and matter effects in neutrino oscillations*, *Phys. Scripta* **T 121** (2005) 57 [hep-ph/0412391] [INSPIRE].

[15] KAMIOKANDE-II collaboration, K. Hirata et al., *Experimental study of the atmospheric neutrino flux*, *Phys. Lett.* **B 205** (1988) 416 [INSPIRE].

[16] MACRO collaboration, M. Ambrosio et al., *Measurement of the atmospheric neutrino induced upgoing muon flux using MACRO*, *Phys. Lett.* **B 434** (1998) 451 [hep-ex/9807005] [INSPIRE].

[17] Soudan-2 collaboration, W. Allison et al., *Neutrino oscillation effects in Soudan-2 upward-stopping muons*, *Phys. Rev.* **D 72** (2005) 052005 [hep-ex/0507068] [INSPIRE].

[18] K2K collaboration, M. Ahn et al., *Measurement of neutrino oscillation by the K2K experiment*, *Phys. Rev.* **D 74** (2006) 072003 [hep-ex/0606032] [INSPIRE].

[19] MINOS collaboration, D. Michael et al., *Observation of muon neutrino disappearance with the MINOS detectors and the NuMI neutrino beam*, *Phys. Rev. Lett.* **97** (2006) 191801 [hep-ex/0607088] [INSPIRE].

[20] MINOS collaboration, P. Adamson et al., *Search for active neutrino disappearance using neutral-current interactions in the MINOS long-baseline experiment*, *Phys. Rev. Lett.* **101** (2008) 221804 [arXiv:0807.2424] [INSPIRE].

[21] OPERA collaboration, *The emulsion technique for short, medium and long baseline $\nu_\mu - \nu_\tau$ oscillation experiments*, INFN-AE-97-06 (1997).

[22] H. Shibuya et al., *Letter of intent: the OPERA emulsion detector for a long-baseline neutrino-oscillation experiment*, CERN-SPSC-97-24 (1997).

[23] OPERA collaboration, *An appearance experiment to search for $\nu_\mu \to \nu_\tau$ oscillations in the CNGS beam: experimental proposal*, CERN-SPSC-2000-028 (2000).

[24] OPERA collaboration, *Status report on the OPERA experiment*, CERN-SPSC-2001-025 (2001).

[25] CHOOZ collaboration, M. Apollonio et al., *Search for neutrino oscillations on a long baseline at the CHOOZ nuclear power station*, *Eur. Phys. J.* **C 27** (2003) 331 [hep-ex/0301017] [INSPIRE].

JHEP11(2013)036

[26] Palo Verde collaboration, A. Piepke, *Final results from the Palo Verde neutrino oscillation experiment*, *Prog. Part. Nucl. Phys.* **48** (2002) 113 [INSPIRE].

[27] T2K collaboration, K. Abe et al., *Indication of electron neutrino appearance from an accelerator-produced off-axis muon neutrino beam*, *Phys. Rev. Lett.* **107** (2011) 041801 [arXiv:1106.2822] [INSPIRE].

[28] DAYA-BAY collaboration, F. An et al., *Observation of electron-antineutrino disappearance at Daya Bay*, *Phys. Rev. Lett.* **108** (2012) 171803 [arXiv:1203.1669] [INSPIRE].

[29] DOUBLE-CHOOZ collaboration, Y. Abe et al., *Indication for the disappearance of reactor electron antineutrinos in the Double CHOOZ experiment*, *Phys. Rev. Lett.* **108** (2012) 131801 [arXiv:1112.6353] [INSPIRE].

[30] RENO collaboration, J. Ahn et al., *Observation of Reactor Electron Antineutrino Disappearance in the RENO experiment*, *Phys. Rev. Lett.* **108** (2012) 191802 [arXiv:1204.0626] [INSPIRE].

[31] Super-Kamiokande collaboration, K. Abe et al., *A measurement of the appearance of atmospheric tau neutrinos by Super-Kamiokande*, *Phys. Rev. Lett.* **110** (2013) 181802 [arXiv:1206.0328] [INSPIRE].

[32] A. Esteban-Pretel, J.W. Valle and P. Huber, *Can OPERA help in constraining neutrino non-standard interactions?*, *Phys. Lett.* **B 668** (2008) 197 [arXiv:0803.1790] [INSPIRE].

[33] M. Blennow, D. Meloni, T. Ohlsson, F. Terranova and M. Westerberg, *Non-standard interactions using the OPERA experiment*, *Eur. Phys. J.* **C 56** (2008) 529 [arXiv:0804.2744] [INSPIRE].

[34] K. Elsener, *The CERN neutrino beam to Gran Sasso. Conceptual technical design*, CERN-98-02 (1998).

[35] R. Bailey et al., *The CERN neutrino beam to Gran Sasso (CNGS)*, CERN-SL-99-034-DI (1999); addendum to report No. CERN-98-0.

[36] *CNGS webpage*, http://proj-cngs.web.cern.ch/proj-cngs.

[37] OPERA collaboration, R. Acquafredda et al., *First events from the CNGS neutrino beam detected in the OPERA experiment*, *New J. Phys.* **8** (2006) 303 [hep-ex/0611023] [INSPIRE].

[38] OPERA collaboration T. Ariga et al., *The detection of neutrino interactions in the emulsion/lead target of the OPERA experiment*, 2009 *JINST* **4** P06020 [arXiv:0903.2973] [INSPIRE].

[39] OPERA collaboration, N. Agafonova et al., *Observation of a first ν_τ candidate in the OPERA experiment in the CNGS beam*, *Phys. Lett.* **B 691** (2010) 138 [arXiv:1006.1623] [INSPIRE].

[40] OPERA collaboration, *Search for $\nu_\mu \to \nu_\tau$ oscillation with the OPERA experiment in the CNGS beam*, *New J. Phys.* **14** (2012) 033017 [arXiv:1107.2594] [INSPIRE].

[41] OPERA collaboration, R. Acquafredda et al., *The OPERA experiment in the CERN to Gran Sasso neutrino beam*, 2009 *JINST* **4** P04018.

[42] T. Adam et al., *The OPERA experiment target tracker*, *Nucl. Instrum. Meth.* **A 577** (2007) 523 [physics/0701153] [INSPIRE].

[43] OPERA collaboration, A. Anokhina et al., *Emulsion sheet doublets as interface trackers for the OPERA experiment*, 2008 *JINST* **3** P07005 [arXiv:0804.1985] [INSPIRE].

JHEP11(2013)036

[44] OPERA collaboration, J. Marteau, *The OPERA global readout and GPS distribution system*, *Nucl. Instrum. Meth.* **A 617** (2010) 291 [arXiv:0906.1494] [INSPIRE].

[45] OPERA collaboration, N. Agafonova et al., *Study of neutrino interactions with the electronic detectors of the OPERA experiment*, *New J. Phys.* **13** (2011) 053051 [arXiv:1102.1882] [INSPIRE].

[46] A. Bertolin et al., *OpCarac: an algorithm for the classification of the neutrino interactions recorded by the OPERA experiment*, OPERA public note n. 100 (2009).

[47] A. Chukanov et al., *Neutrino interaction vertex location with the OPERA electronic detectors*, OPERA public note n. 162 (2013).

[48] A. Ferrari et al., *An updated Monte Carlo calculation of the CNGS neutrino beam*, CERN-AB-Note-2006-038 (2007).

[49] K. Morishima and T. Nakano, *Development of a new automatic nuclear emulsion scanning system, S-UTS, with continuous 3D tomographic image read-out*, 2010 *JINST* **5** P04011.

[50] S. Aoki et al., *The fully automated emulsion analysis system*, *Nucl. Instrum. Meth.* **B 51** (1990) 466 [INSPIRE].

[51] T. Nakano, *Automatic analysis of nuclear emulsion*, Ph.D. thesis, Nagoya University, Japan (1997).

[52] G. Rosa, A. Di Bartolomeo, G. Grella and G. Romano, *Automatic analysis of digitized TV images by a computer driven optical microscope*, *Nucl. Instrum. Meth.* **A 394** (1997) 357 [INSPIRE].

[53] N. Armenise et al., *High-speed particle tracking in nuclear emulsion by last-generation automatic microscopes*, *Nucl. Instrum. Meth.* **A 551** (2005) 261 [INSPIRE].

[54] L. Arrabito et al., *Hardware performance of a scanning system for high speed analysis of nuclear emulsions*, *Nucl. Instrum. Meth.* **A 568** (2006) 578 [physics/0604043] [INSPIRE].

[55] L. Arrabito et al., *Track reconstruction in the emulsion-lead target of the OPERA experiment using the ESS microscope*, 2007 *JINST* **2** P05004.

[56] I. Kreslo et al., *High-speed analysis of nuclear emulsion films with the use of dry objective lenses*, 2008 *JINST* **3** P04006.

[57] M. De Serio et al., *High precision measurements with nuclear emulsions using fast automated microscopes*, *Nucl. Instrum. Meth.* **A 554** (2005) 247.

[58] C. Bozza et al., *An integrated system for large scale scanning of nuclear emulsions*, *Nucl. Instrum. Meth.* **A 703** (2013) 204.

[59] T. Fukuda et al., *The analysis of interface emulsion detector for the OPERA experiment in JAPAN scanning facility*, 2010 *JINST* **5** P04009.

[60] J. Yoshida et al., *Development and utilization of "Plate Changer" system for neutrino interaction locations in OPERA emulsion target*, 2013 *JINST* **8** P02009.

[61] S. Balestra et al., *A fast automatic plate changer for the analysis of nuclear emulsions*, *Nucl. Instrum. Meth.* **A 716** (2013) 96.

[62] T. Fukuda et al. *Automatic scanning of nuclear emulsions with wide angle acceptance for nuclear fragment detection*, 2013 *JINST* **8** P01023.

JHEP11(2013)036

[63] A. Ben Dhahbi, *Nuclear fragmentation study in hadron interactions within the OPERA experiment*, Ph.D. thesis, Bern Univiversity, Bern, Switzerland (2013), available online.

[64] OPERA collaboration, N. Agafonova et al., *Momentum measurement by the multiple Coulomb scattering method in the OPERA lead emulsion target*, *New J. Phys.* **14** (2012) 013026 [arXiv:1106.6211] [INSPIRE].

[65] A. Ariga et al., *A method to search for short-lived particle decays in the* OPERA *experiment*, OPERA public note n. 128 (2011).

[66] CHORUS collaboration. A. Kayis-Topaksu et al., *Measurement of charm production in neutrino charged-current interactions*, *New J. Phys.* **13** (2011) 093002.

[67] OPERA collaboration, N. Agafonova et al., *Neutrino induced charm production in the OPERA experiment*, in preparation.

[68] L. Arrabito et al., *Electron/pion separation with an emulsion cloud chamber by using a neural network*, 2007 *JINST* **2** P02001 [physics/0701192] [INSPIRE].

[69] OPERA collaboration, N. Agafonova et al., *Search for $\nu_\mu \to \nu_e$ oscillations with the OPERA experiment in the CNGS beam*, *JHEP* **07** (2013) 004 [*Addendum ibid.* **1307** (2013) 085] [arXiv:1303.3953] [INSPIRE].

[70] E.L. Berger et al., *The minimum invariant mass — A technique for heavy quark searches at collider energy*, *Phys. Lett.* **B 140** (1984) 259 [INSPIRE].

[71] A. Di Crescenzo, *Search for $\nu_\mu \to \nu_\tau$ oscillations in the* OPERA *experiment*, Ph.D. thesis, Università di Napoli, Napoli, Italy (2013), available online.

[72] A. Fassò et al. *FLUKA: a multi-particle transport code*, CERN-2005-10 (2005).

[73] *FLUKA web page*, http://www.fluka.org/fluka.php.

[74] *CNGS neutrino flux calculation webpage*, http://www.mi.infn.it/∼psala/Icarus/cngs.html.

[75] D. Autiero, *The OPERA event generator and the data tuning of nuclear re-interactions*, *Nucl. Phys. Proc. Suppl.* **B 139** (2005) 253.

[76] C. Andreopoulos et al., *The GENIE neutrino Monte Carlo generator*, *Nucl. Instrum. Meth.* **A 614** (2010) 87 [arXiv:0905.2517] [INSPIRE].

[77] Particle Data Group collaboration, K. Nakamura et al., *Review of particle physics*, *J. Phys.* **G 37** (2010) 075021 [INSPIRE].

[78] CHORUS collaboration, A. Kayis-Topaksu et al., *Associated charm production in neutrino-nucleus interactions*, *Eur. Phys. J.* **C 52** (2007) 543 [arXiv:0708.2820] [INSPIRE].

[79] R. Rescigno, *The neutrino interaction analysis chain in OPERA*, Ph.D. thesis, Università di Salerno, Salerno, Italy (2011), available online.

[80] S.M. Stellacci, *Study of the hadronic current in the neutrino interactions of the OPERA experiment*, Ph.D. thesis, Università di Salerno, Salerno, Italy (2013), available online.

[81] H. Ishida, *Study of hadron backgrounds for τ-decay events in neutrino oscillation experiments*. Ph.D. Thesis, Toho University, Tokyo, Japan (2013).

[82] H. Ishida et al., *Study of hadron interactions in an ECC brick*, in preparation.

[83] R. Brun et al., *GEANT 3.21*, CERN Report DD/EE/84-1 (1984).

JHEP11(2013)036

The OPERA collaboration

N. Agafonova,[a] A. Aleksandrov,[b] A. Anokhina,[c] S. Aoki,[d] A. Ariga,[e] T. Ariga,[e] T. Asada,[x] D. Autiero,[f] A. Badertscher,[g] A. Ben Dhahbi,[e] D. Bender,[z] A. Bertolin,[h] C. Bozza,[i] R. Brugnera,[h,j] G. Brunetti,[e] B. Büttner,[k] S. Buontempo,[b] L. Chaussard,[f] M. Chernyavskiy,[l] V. Chiarella,[m] A. Chukanov,[n] L. Consiglio,[b] N. D'Ambrosio,[o] P. Del Amo Sanchez,[t] G. De Lellis,[b,p] M. De Serio,[q] A. Di Crescenzo,[b,p] D. Di Ferdinando,[r] N. Di Marco,[o] S. Dmitrievski,[n] M. Dracos,[s] D. Duchesneau,[t] S. Dusini,[h] J. Ebert,[k] A. Ereditato,[e] J. Favier,[t] T. Ferber,[k,1] R. A. Fini,[q] T. Fukuda,[u] A. Garfagnini,[h,j] G. Giacomelli,[v,r] C. Goellnitz,[k] J. Goldberg,[y] Y. Gornushkin,[n] G. Grella,[i] F. Grianti,[m,w] A. M Guler,[z] C. Gustavino,[aa] C. Hagner,[k] K. Hakamata,[x] T. Hara,[d] T. Hayakawa,[x] M. Hierholzer,[k,2] A. Hollnagel,[k] B. Hosseini,[b,p] H. Ishida,[u] K. Ishiguro,[x] M. Ishikawa,[x] K. Jakovcic,[aa] C. Jollet,[s] C. Kamiscioglu,[z,ak] M. Kamiscioglu,[z] T. Katsuragawa,[x] H. Kawahara,[x] J. Kawada,[e] J. H. Kim,[ab,ag] S. H. Kim,[ab,ag,3] M. Kimura,[e] N. Kitagawa,[x] B. Klicek,[aa] K. Kodama,[ac] M. Komatsu,[x] U. Kose,[h] I. Kreslo,[e] A. Lauria,[b,p] J. Lenkeit,[k] A. Ljubicic,[aa] A. Longhin,[m] P. Loverre,[ad,aa] A. Malgin,[a] G. Mandrioli,[r] J. Marteau,[f] T. Matsuo,[u] V. Matveev,[a] N. Mauri,[v,r] E. Medinaceli,[h,j] A. Meregaglia,[s] P. Migliozzi,[b] S. Mikado,[u] A. Minotti,[ad,4] M. Miyanishi,[x] E. Miyashita,[x] P. Monacelli,[ag] M. C. Montesi,[b,p] K. Morishima,[x] M. T. Muciaccia,[q,ae] N. Naganawa,[x] T. Naka,[x] M. Nakamura,[x] T. Nakano,[x] Y. Nakatsuka,[x] K. Niwa,[x] S. Ogawa,[u] N. Okateva,[l] A. Olshevsky,[n] T. Omura,[x] K. Ozaki,[d] A. Paoloni,[m] B. D. Park,[ab,5] I. G. Park,[ab] A. Pastore,[q] L. Patrizii,[r] E. Pennacchio,[f] H. Pessard,[t] C. Pistillo,[e] D. Podgrudkov,[c] N. Polukhina,[l] M. Pozzato,[v,r] K. Pretzl,[e] F. Pupilli,[o] R. Rescigno,[i] M. Roda,[h] T. Roganova,[c] H. Rokujo,[x] G. Rosa,[ad,aa] I. Rostovtseva,[aj] A. Rubbia,[g] A. Russo,[b] O. Ryazhskaya,[a] O. Sato,[x] Y. Sato,[ah] A. Schembri,[o] W. Schmidt-Parzefall,[k] I. Shakiryanova,[a] T. Schcedrina,[l,b] A. Sheshukov,[n] H. Shibuya,[u] T. Shiraishi,[x] G. Shoziyoev,[c] S. Simone,[q,ae] M. Sioli,[v,r] C. Sirignano,[h,j] G. Sirri,[r] M. Spinetti,[m] L. Stanco,[h] N. Starkov,[l] S.M. Stellacci,[i] M. Stipcevic,[aa] T. Strauss,[e] P. Strolin,[b,p] K. Suzuki,[x] S. Takahashi,[d] M. Tenti,[v,r] F. Terranova,[m,af] V. Tioukov,[b] P. Tolun,[z,6] S. Tufanli,[e] P. Vilain,[ai] M. Vladimirov,[l] L. Votano,[m] J. L. Vuilleumier,[e] G. Wilquet,[ai] B. Wonsak,[k] C.S. Yoon,[ab] J. Yoshida,[x] M. Yoshimoto,[x] Y. Zaitsev,[aj] S. Zemskova,[n] A. Zghiche[t]

[a] *INR Institute for Nuclear Research, Russian Academy of Sciences RUS-117312, Moscow, Russia*
[b] *INFN Sezione di Napoli, I-80125 Napoli, Italy*
[c] *SINP MSU-Skobeltsyn Institute of Nuclear Physics, Lomonosov Moscow State University, RUS-119992 Moscow, Russia*
[d] *Kobe University, J-657-8501 Kobe, Japan*
[e] *Albert Einstein Center for Fundamental Physics, Laboratory for High Energy Physics (LHEP), University of Bern, CH-3012 Bern, Switzerland*
[f] *IPNL, Université Claude Bernard Lyon 1, CNRS/IN2P3, F-69622 Villeurbanne, France*
[g] *ETH Zurich, Institute for Particle Physics, CH-8093 Zurich, Switzerland*
[h] *INFN Sezione di Padova, I-35131 Padova, Italy*
[i] *Dip. di Fisica dell'Univ. di Salerno and "Gruppo Collegato" INFN, I-84084 Fisciano (SA) Italy*
[j] *Dipartimento di Fisica dell'Università di Padova, I-35131 Padova, Italy*
[k] *Hamburg University, D-22761 Hamburg, Germany*
[l] *LPI-Lebedev Physical Institute of the Russian Academy of Sciences, 119991 Moscow, Russia*
[m] *INFN-Laboratori Nazionali di Frascati dell'INFN, I-00044 Frascati (Roma), Italy*
[n] *JINR-Joint Institute for Nuclear Research, RUS-141980 Dubna, Russia*
[o] *INFN-Laboratori Nazionali del Gran Sasso, I-67010 Assergi (L'Aquila), Italy*
[p] *Dipartimento di Scienze Fisiche dell'Università Federico II di Napoli, I-80125 Napoli, Italy*
[q] *INFN Sezione di Bari, I-70126 Bari, Italy*

JHEP11(2013)036

[r] INFN Sezione di Bologna, I-40127 Bologna, Italy
[s] IPHC, Université de Strasbourg, CNRS/IN2P3, F-67037 Strasbourg, France
[t] LAPP, Université de Savoie, CNRS IN2P3, F-74941 Annecy-le-Vieux, France
[u] Toho University, J-274-8510 Funabashi, Japan
[v] Dipartimento di Fisica dell'Università di Bologna, I-40127 Bologna, Italy
[w] Università degli Studi di Urbino 'Carlo Bo', I-61029 Urbino, Italy
[x] Nagoya University, J-464-8602 Nagoya, Japan
[y] Department of Physics, Technion, IL-32000 Haifa, Israel
[z] METU Middle East Technical University, TR-06531 Ankara, Turkey
[aa] IRB-Rudjer Boskovic Institute, HR-10002 Zagreb, Croatia
[ab] Gyeongsang National University, ROK-900 Gazwa-dong, Jinju 660-701, Korea
[ac] Aichi University of Education, J-448-8542 Kariya (Aichi-Ken), Japan
[ad] Dipartimento di Fisica dell'Università di Roma 'La Sapienza' and INFN, I-00185 Roma, Italy
[ae] Dipartimento di Fisica dell'Università di Bari, I-70126 Bari, Italy
[af] Dipartimento di Fisica dell'Università di Milano-Bicocca, I-20126 Milano, Italy
[ag] Dipartimento di Fisica dell'Università dell'Aquila and INFN, I-67100 L'Aquila, Italy
[ah] Utsunomiya University, J-321-8505 Tochigi-Ken, Utsunomiya, Japan
[ai] IIHE, Université Libre de Bruxelles, B-1050 Brussels, Belgium
[aj] ITEP-Institute for Theoretical and Experimental Physics, RUS-317259 Moscow, Russia
[ak] Ankara University, TR-06100 Ankara, Turkey
[al] INFN Sezione di Roma, I-00185 Roma, Italy

[1] Now at Deutsches Elektronen Synchrotron (DESY), 22607 Hamburg, Germany
[2] Now at LHEP, Univ. of Bern, CH-3012 Bern, Switzerland
[3] Now at Kyungpook National Univ., 80 Daehakro, Bukgu, Daegu, Rep. of Korea
[4] Now at IPHC, Université de Strasbourg, CNRS/IN2P3, F-67037 Strasbourg, France
[5] Now at Samsung Changwon Hospital, Sungkyunkwan Univ., 158 Palyongro, MasanHoiwongu, Changwon, Rep. of Korea
[6] Deceased

JHEP11(2013)036